

Soft Matter

Accepted Manuscript



This is an *Accepted Manuscript*, which has been through the Royal Society of Chemistry peer review process and has been accepted for publication.

Accepted Manuscripts are published online shortly after acceptance, before technical editing, formatting and proof reading. Using this free service, authors can make their results available to the community, in citable form, before we publish the edited article. We will replace this *Accepted Manuscript* with the edited and formatted *Advance Article* as soon as it is available.

You can find more information about *Accepted Manuscripts* in the [Information for Authors](#).

Please note that technical editing may introduce minor changes to the text and/or graphics, which may alter content. The journal's standard [Terms & Conditions](#) and the [Ethical guidelines](#) still apply. In no event shall the Royal Society of Chemistry be held responsible for any errors or omissions in this *Accepted Manuscript* or any consequences arising from the use of any information it contains.

COMMUNICATION

Real-space Evidence of the Equilibrium Ordered Bicontinuous Double Diamond Structure of Diblock Copolymer

Cite this: DOI: 10.1039/x0xx00000x

Received 00th January 2012,
Accepted 00th January 2012C. Y. Chu,^a X. Jiang,^b H. Jinnai,^{*b} R. Y. Pei,^a W. F. Lin,^c J. C. Tsai^c and H. L. Chen^{*a}

DOI: 10.1039/x0xx00000x

www.rsc.org/

Ordered bicontinuous double diamond (OBDD) has long been believed to be an unstable ordered network nanostructure relative to ordered bicontinuous double gyroid (OBDG) for diblock copolymers. Using electron tomography, here we present the first real-space observation of the thermodynamically stable OBDD structure in a diblock copolymer composed of a stereoregular block, syndiotactic polypropylene-block-polystyrene (sPP-*b*-PS), in which the sPP tetrapods interconnected into a bicontinuous network with $Pn\bar{3}m$ symmetry. The OBDD structure underwent a thermally reversible order-order transition (OOT) to OBDG upon heating, and the transition was accompanied with a slight reduction of domain spacing, as demonstrated both experimentally and theoretically. The thermodynamic stability of the OBDD structure was attributed to the ability of the configurationally regular sPP block to form helical segments even above its melting point, as the reduction of internal energy associated with the helix formation may effectively compensate the greater packing frustration in OBDD relative to that in the tripod of OBDG.

Nanotechnology based on the materials with the structure characteristics on nanoscale dimension has advanced the development of various areas, including opto-electronics, biomedicines, and energy storage and transmission.¹⁻⁷ Great strides have been made in nanotechnological research by exploiting the ordered network nanostructures which contains two or more distinctly periodic hyperbolic surfaces that continuously percolate through the specimen in all three dimensions.⁸ As a result of the spatial continuity of domains in the network structures,⁹⁻¹² the materials may exhibit superior mechanical properties in comparison to that derived from the typical structure-directing agent using

lamellar or cylindrical morphologies. With the characteristic of continuity of channels complemented by the high surface area of the interfaces, the ordered network nanostructures could be potentially utilized in catalysts,¹³⁻¹⁵ 3D photonic crystals,^{16,17} nanofiltration membranes,^{18,19} bulk heterojunction solar cells,²⁰⁻²³ supercapacitors,²⁴ and electrodes.²⁵

Molecular self-assembly of soft matter is an effective approach to create a wide variety of long-range ordered nanostructures. The existing ordered network nanostructures of soft materials include ordered bicontinuous double gyroid (OBDG),²⁶⁻²⁸ single network gyroid,²⁹ ordered tricontinuous double diamond (OTDD),³⁰⁻³² *Fddd* network,^{33,34} and *Pnna* network.³⁵ These ordered networks are all characterized by three-fold coordinated network lattices.³⁶ In contrast to the commonly observed OBDG structure which is characterized by the tripod microdomains interconnected with $Ia\bar{3}d$ symmetry, another bicontinuous structure, i.e., ordered bicontinuous double diamond (OBDD), formed by the tetrapod organized in $Pn\bar{3}m$ symmetry has only been observed in complex fluids such as lipid-water systems³⁷ and surfactants.^{38,39} In the case of diblock copolymers, OBDD has long been considered as an unstable structure relative to OBDG until our recent study which disclosed the existence of a thermodynamically stable OBDD structure in a diblock copolymer composed of a configurationally regular block, syndiotactic polypropylene-block-polystyrene (sPP-*b*-PS).⁴⁰ Moreover, the OBDD structure formed in this system was found to undergo an order-order transition (OOT) to OBDG upon heating. The discovery of the OBDD structure in diblock copolymer with relatively high molecular weight expands the morphological window of ordered network nanostructure with large domain size.

In the previous study, the OBDD structure was revealed in reciprocal space by the powder pattern of small angle X-ray scattering (SAXS) using an in-house SAXS instrument equipped with the detector of relatively low resolution, which hampered the precise identification of some important features of the OBDD-OBDG transition. In this study, we present the first real-space evidence of the OBDD

structure in the sPP-*b*-PS system to corroborate with the high-resolution SAXS result collected using a synchrotron radiation source and a high-resolution detector that allows the slight change of domain spacing across the OOT, which was not identified previously, to be clearly resolved. Here we start with the elucidation of the OOT by means of the high-resolution SAXS profiles and a geometric analysis to reveal a difference in domain spacing between the two bicontinuous structures. Then, the 3D image obtained from the electron tomography⁴¹ will be presented to affirmatively show the formation of OBDD structure, in which the sPP tetrapod microdomains interconnect to form a bicontinuous network with $Pn\bar{3}m$ symmetry.

The sPP-*b*-PS diblock copolymer ($M_{n,sPP} = 6800$, $M_{n,PS} = 9400$, $PDI = M_w/M_n = 1.19$) studied here with the volume fraction of 0.46 of the sPP block in the melt state was prepared in two steps according to the procedure reported in the literature.⁴² The as-cast film of the diblock copolymer was prepared in the same way as that reported in our previous study.⁴⁰ The morphology of the sPP-*b*-PS was probed by SAXS performed at the Endstation BL23A1 of the National Synchrotron Radiation Research Center (NSRRC), Taiwan. The energy of the X-ray source and the sample-to-detector distance were 10 keV and 1850 mm, respectively. The scattering signals were collected by a PILATUS 1M-F detector which is a hybrid pixel array detector with over one million pixels operated in single photon counting mode.⁴³ The scattering intensity profile was output as the plot of the scattering intensity (I) versus the magnitude of the scattering vector, $q = (4\pi/\lambda) \sin(\theta/2)$ (θ = scattering angle). The SAXS profiles were corrected for the incident beam intensity, the background, and the detector sensitivity.

For the real-space observations of the OBDD morphology by electron tomography, the ultrathin section with the thickness of 150 nm was prepared by microtome at cryogenic condition using diamond knife (UltraCut7, Leica), and transferred to Formvar covered copper grid. The ultrathin section was stained with the vapor of RuO₄ crystal at 300 Pa for 30 min, followed by coating 15 nm amorphous carbon layers on both top and bottom surfaces to prevent from being charged on the surface during image acquisition. Au colloid nanoparticles with 5 nm diameter in aqueous solution were dropped on both sides of the grid as fiducial markers. Electron tomography was carried out using a JEM-2200FS microscope (JEOL, Ltd., Japan) operated at 200 kV and equipped with in-column energy filter. A series of bright-field micrographs were acquired at tilt angles in the range of $\pm 66^\circ$ at an angular interval of 1° . The tilt series of the micrographs were then aligned by the tracking fiducial markers. The aligned micrographs were constructed using simultaneous iterative reconstruction techniques (SIRT) in IMOD.^{44,45} The OBDD microdomains in the reconstructed tomogram was further manually segmented. In order to show the featured morphology of OBDD structure, the corresponding 3D visualization image and 3D thinned image were generated in AVIZO using surface rendering and skeleton subsequently. The function of “skeletonization” in the software provides automatic and semi-automatic tools for quantitative study of filament networks, and the satisfactory thinning was judged by examining the thinned images by the naked eyes.

Fig. 1a shows the temperature-dependent SAXS profiles of the sPP-*b*-PS film obtained in a heating cycle. The calculated SAXS curves associated with OBDD and OBDG structures are shown in Fig. S1 of the Supplementary Information. The SAXS profile observed at 30 °C shows five diffraction peaks with the position ratios consistent with that prescribed by the OBDD structure (see Fig. S1). It is noted that a small peak locating at ca. 0.18 nm^{-1} is observable in the SAXS profiles collected between 30 °C and 125 °C. This peak may be associated with the morphology formed by the crystallization of sPP

during the solvent casting process, as it vanishes above 125 °C where the sPP crystals are completely melted (see Figure S2 of the Supplementary Information for demonstrating the melting of sPP crystals above 125 °C). When the copolymer is heated to 175 °C, the position of the second-order relative to that of the first-order peak shifts clearly from $(3/2)^{1/2}$ to $(4/3)^{1/2}$, and the scattering pattern becomes consistent with that associated with the OBDG phase. The coexistence of both the OBDD and OBDG structures is found across the OOT region at $175 \leq T \text{ (}^\circ\text{C)} \leq 185$. An important finding that was not identified in our previous SAXS result is the obvious difference between the primary peak position of OBDD ($q_{110} = 0.247 \text{ nm}^{-1}$) and that of OBDG ($q_{211} = 0.261 \text{ nm}^{-1}$) across the OOT, as demonstrated in Fig. 1b. Upon cooling, the OBDG structure transforms back to OBDD and the primary peak also shifts back to the position originally found for OBDD, as revealed in Fig. S1. This observation essentially gives us a hint that the OOT is associated with a certain kind of epitaxial transition. The origin of the difference in primary peak position between OBDD and OBDG will be elucidated below by deriving the characteristic domain spacings of these two bicontinuous structures.

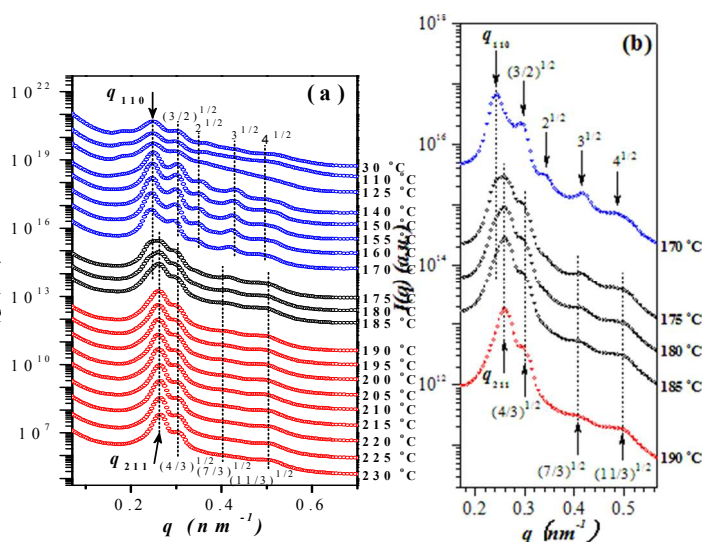


Fig. 1 (a) Temperature-dependent SAXS profiles of the sPP-*b*-PS obtained in a heating cycle. The primary peak positions of OBDD ($q_{110} = 0.247 \text{ nm}^{-1}$) and OBDG ($q_{211} = 0.261 \text{ nm}^{-1}$) structures are indicated by the arrows. (b) The expanded view of the SAXS profiles over the temperature range of 170 to 190 °C to show the coexistence of the primary peaks of OBDD and OBDG phases across the OOT region from 175 to 185 °C.

It has been reported that the characteristic spacing d_{hkl} of OBDD or OBDG structure can be calculated by:^{26,46}

$$d_{hkl} = \frac{a_i}{\sqrt{h^2 + k^2 + l^2}} \quad (1)$$

where a is the lattice parameter of the cubic unit cell with $i = D$ or G corresponding to the OBDD or OBDG structure, respectively, and (hkl) are the Miller indices of the allowed diffractions. By substituting (hkl) index of the primary peak of OBDD and OBDG, i.e., (110) and (211), respectively into eq 1, the domain spacings of these two structures are given by $d_{110} = \frac{a_D}{\sqrt{2}}$ and $d_{211} = \frac{a_G}{\sqrt{6}}$. To quantitatively compare the domain spacing between OBDD and OBDG across the OOT, the ratio $\frac{d_{110}}{d_{211}} = \sqrt{3} \times \frac{a_D}{a_G}$ is calculated.

The term $\frac{a_D}{a_G}$ is derived by the following steps by considering the transformation from tetrapod into tripod assuming the conservation

of volume of the microdomains due to low thermal expansion of the sPP-*b*-PS diblock copolymer studied (see Fig. S3 of the Supporting Information).⁴⁷⁻⁵⁰ Previous studies have reported that the transformation from (6,4) net of D surface in the OBDD phase into (10,3) net of G surface in the OBDG phase can be achieved by pulling apart a tetrahedral vertex to form two trigonal vertices.⁵¹ Consequently, the equation based on the conservation of volume can be expressed as

$$4 \times \left(\frac{1}{2}V'_D\right) = 6 \times \left(\frac{1}{2}V'_G\right) \quad (2)$$

where V'_D and V'_G are given by the sum of the volume of one connecting domain with hyperbolic surface (formed by sPP block in the present system) formed between two nodes and the volume of two quarters or two one-third of the node lying at the both ends of the connecting microdomain in the OBDD and OBDG structure, respectively. The microdomain with hyperbolic surface connecting the nodes is schematically illustrated in Fig. S4 of the Supplementary Information.

On the other hand, the total volume of the microdomains in a unit cell can be represented as

$$f_i \times a_i^3 = N_i \times V'_i \quad (3)$$

where f_i is the volume fraction of the sPP block and N_i is the number of the connecting domains in a unit cell. i refers to the OBDD or OBDG structure.

According to the assumption of volume conservation, f_i remains unchanged between OBDD and OBDG phase; therefore, through the uses of eq 3 and eq 2, $\frac{a_D}{a_G}$ can be expressed in terms of the ratio of the number of connecting microdomains in an OBDD and an OBDG unit cell, viz.

$$\left(\frac{a_D}{a_G}\right)^3 = \frac{N_D}{N_G} \times \frac{3}{2} \quad (4)$$

The term of N_i in either OBDD or OBDG structure can be further replaced by the number of tetrapod or tripod nodes via

$$N_{node,D} = \frac{N_D - 1}{3} \quad (5)$$

$$N_{node,G} = \frac{N_G - 1}{2} \quad (6)$$

where $N_{node,i}$ is the number of nodes forming the tetrapod and tripod networks in the unit cell of OBDD and OBDG phase. Based on the combination of eq 4, eq 5 and eq 6, the ratio of the domain spacing between OBDD and OBDG, i.e., $\frac{d_{110}}{d_{211}}$, can be written in terms of a_i and $N_{node,i}$ as

$$\frac{d_{110}}{d_{211}} = \sqrt{3} \times \sqrt[3]{\frac{3}{2}} \times \sqrt[3]{\frac{3N_{node,D} + 1}{2N_{node,G} + 1}} \quad (7)$$

The theoretical numbers of nodes in a unit cell of OBDD and OBDG, i.e., $N_{node,D}$ and $N_{node,G}$, are 2 and 16, respectively.^{52,54}

Consequently, the value of $\frac{d_{110}}{d_{211}}$ ratio calculated from eq 7 is 1.18.

Comparing the calculated value of $\frac{d_{110}}{d_{211}}$ with the experimentally observed value may offer a convenient way to examine if the observed OBDD-OBDG transition deviates from the thermodynamically equilibrium process. From Fig. 1, the experimental value of $\frac{d_{110}}{d_{211}}$ ratio can be calculated from the peak positions via $\frac{d_{110}}{d_{211}} = \frac{q_{211}}{q_{110}}$, which yields the value of 1.06. This value is smaller than that predicted theoretically by eq 7. The discrepancy may imply that the domain spacings of OBDD and/or OBDG structure formed in the present sPP-*b*-PS system may not correspond to the values associated with the lowest free energy state, although the transition between them is thermodynamically driven,⁴⁰ because the annealing time (i.e., 5 min) at each temperature for the synchrotron SAXS experiment was short.

To visualize the OBDD structure in real space, the as-cast sample was cut into the ultrathin section for observation by TEM. Fig. 2

displays an observed 2D TEM micrograph. The observed image of wagon-wheel lattice⁵⁵ in Region b and another two images in Region c and d may be simulated by the projections from the [111], [211] and [1-11] directions of the OBDD lattice, as also displayed in Fig. 2. However, it has been reported that the 2D projection of the tetrapods in OBDD structure was quite similar to that of the tripods in OBDG phase,⁵⁴ and this makes it difficult to distinguish between these two bicontinuous structures only by the 2D TEM image. Consequently, electron tomography was conducted in this study to obtain the unambiguous real-space evidence of the OBDD structure.

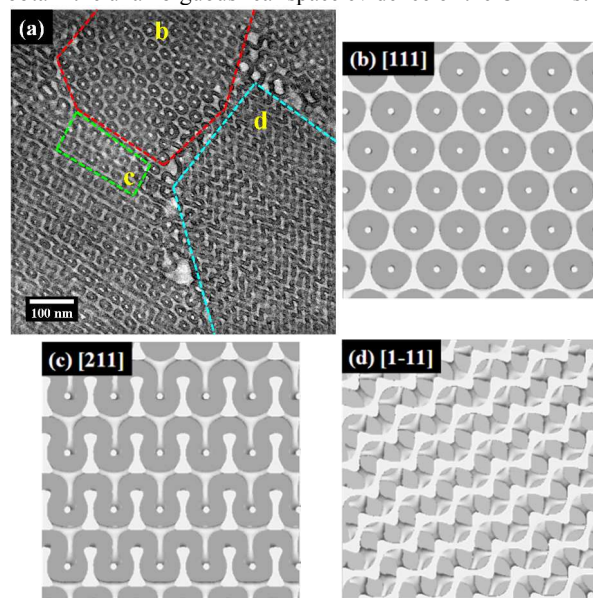


Fig. 2 (a) A 2D TEM image of the nanostructure formed by sPP-*b*-PS. The PS phase appears as the dark region in the micrograph while sPP phase corresponds to the bright region. The TEM image shows the characteristic views of the wagon-wheel lattice and another typical images of OBDD, which can be simulated by the projections from the [111], [211] and [1-11] directions, respectively, as displayed in (b-d).

To construct the 3D image, a series of micrographs of the area showing the wagon-wheel image in Fig. 2 were collected with the tilt angles of $\pm 66^\circ$, followed by combining all the 2D micrographs to generate the 3D image. Fig. 3a shows the representative 3D image of the structure in the as-cast sPP-*b*-PS and the lower magnification (to cover a larger area) of the 3D image is shown in Fig. S5 of the Supplementary Information. It can be seen that the tetrapod microdomains composed of the sPP block (shown in gray color) are interconnected with $Pn\bar{3}m$ symmetry and (6,4) nets, thereby revealing the double-diamond lattice, a model proposed previously by Thomas et al.⁵³ and Hasegawa et al.⁵⁴ To show the network morphology more clearly, the 3D thinning^{56,57} of the microdomains was performed and the result is shown in Fig. 3b. The tetrapod connection characteristic to OBDD can be lucidly observed in the thinning image where the inclined angle between two adjacent pods is very close to 109.5° , consistent with the value reported.⁵³ The 3D TEM image coupled with the SAXS results thus offer a solid evidence for the existence of OBDD structure in the present diblock copolymer.

OBDD structure has never been observed among the conventional diblock copolymers, where OBDG has always been considered as the equilibrium bicontinuous structure. As a result, the configurational regularity of the sPP block in sPP-*b*-PS could be responsible for the stability of OBDD structure. Previous self-consistent field theory calculation indicated that the mean curvature

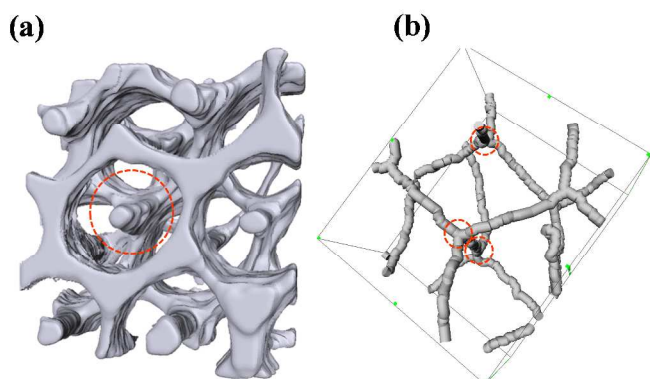


Fig. 3 (a) 3D TEM image of the OBDD structure in the sPP-*b*-PS where the microdomains composed of the sPP block (displayed in gray color) constructs the double-diamond lattice with the tetrapod microdomains connected with $Pn\bar{3}m$ symmetry and (6,4) nets. The image shown in (b) reveals the 3D thinned image of the unit cell of OBDD structure.

of the OBDD microdomains shows a significant deviation from the constant mean curvature; therefore, the degree of packing frustration due to the nonuniform stretching of the block chains forming the domains in OBDD is significantly higher than that associated with OBDG.^{58,59} Later, a more rigorous definition of the distribution of local channel radii in bicontinuous mesophases based on the concept of a medial surface (i.e., a hypothetical surface lying in the middle of microdomains), was used to quantify the degree of packing frustration of the block chains, which depicted that the OBDG geometry emerges as the most homogeneous bicontinuous form with the smallest heterogeneity of channel radii compared to the OBDD surface.⁶⁰ On the other hand, the specific surface area of OBDD was calculated to be smaller than that of OBDG.^{29,60}

In the case of the conventional diblock coils obeying Gaussian statistics, the effect of packing frustration always outweighs the interfacial energy, such that OBDG is always favored. The situation may be different in stereoregular diblock copolymers. It is known that the stereoregular polymers adopt helical conformation in the crystalline state, and the helical segments still persist at temperature above the melting point due to strong intra-chain coupling. The population of the helical segments decreases with increasing temperature, as has been demonstrated for the present sPP-*b*-PS in the previous study.⁴⁰ The ability of the stereoregular block to form helical segments in the melt state may thus exert a significant impact on the microdomain structure. In the previous study, we proposed that the helical segments in the sPP microdomains might form locally ordered regions and the reduction of energy associated with the formation of these regions may compensate the high packing frustration of the OBDD structure, such that OBDD could be more stable than OBDG due to lower interfacial energy. However, the fact that these ordered regions are not detectable by X-ray scattering implies that they are of very small size or low content if they do exist. In this case, it appears implausible that the reduction of total energy due to the formation of the ordered regions is sufficient to compensate the high entropic penalty arising from packing frustration.

Here we evoke an alternative model which is more plausible in the sense that it does not resort to the formation of the locally ordered regions by the helical segments of sPP block. Fig. 4b schematically illustrates the chain stretching of the stereoregular blocks to reach a common medial surface from the domain interface, while the case of the conventional block chains is shown in Fig. 4a. Here we still assert that the entropic loss of the overly stretched sPP blocks may

be compensated by the reduction of internal energy on forming helical segments, but now the population of helical segments in the chain depends on its degree of stretching. As suggested in Fig. 4b, the more stretched sPP chains in the OBDD domains may form more helical segments compared to the relaxed blocks, and the reduction of internal energy arising from the formation of more helical segments in the block chains may compensate the entropic loss. That is, the development of more helical segments in the sPP block may help alleviate the free energy penalty of packing frustration; therefore, OBDD becomes the stable structure due to its lower interfacial energy.

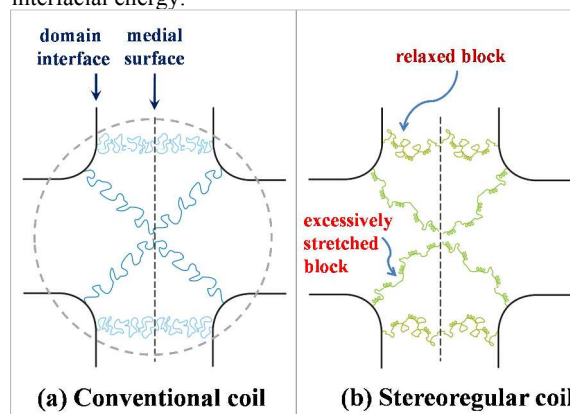


Fig. 4 Schematic illustration of the comparison between (a) conventional coil block and (b) stereoregular block in bicontinuous channels via the medial surface construction. The dashed circle marks the tetrapod microdomains.

In conclusion, we have reported the first real-space evidence of the OBDD structure formed in the diblock copolymer composed of a stereoregular block. The present work opens up possibilities for creating this kind of tetrapod network nanostructure in neat diblock copolymer systems and also provides new opportunities for application of such materials in nanotechnology by exploiting configurational regularity of polymer.

Acknowledgements

This research was supported from the Ministry of Science and Technology, Taiwan, under grant MOST 102-2221-E-007-136-MY3.

Notes and references

^a Department of Chemical Engineering and Frontier Research Center on Fundamental and Applied Sciences of Matters, National Tsing Hua University, Hsin-Chu 30013, Taiwan. E-mail: hlchen@che.nthu.edu.tw

^b Institute for Materials Chemistry and Engineering (IMCE), Kyushu University, 744 Motooka, Nishi-ku, Fukuoka 819-0395, Japan. E-mail: hjinnai@cstf.kyushu-u.ac.jp

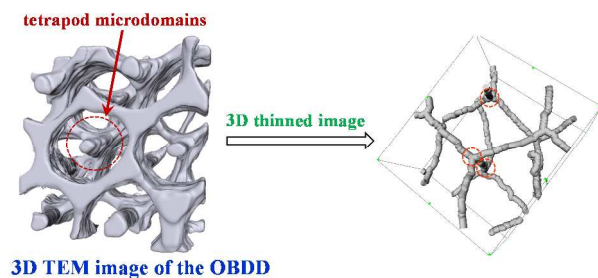
^c Department of Chemical Engineering, National Chung Cheng University, Chia-Yi 62102, Taiwan

Electronic Supplementary Information (ESI) available: Fig. S1, S2, S3 S4 and S5. See DOI: 10.1039/c000000x/

- 1 C. Bai and M. Liu, *Nano Today*, 2012, 7, 258.
- 2 D. Jariwala, V. K. Sangwan, L. J. Lauhon, T. J. Marks and M. C. Hersam, *Chem. Soc. Rev.* 2013, 42, 2824.

- 3 P. J. Vikesland and K. R. Wigginton, *Environ. Sci. Technol.* 2010, **44**, 3656.
- 4 K. E. Sapsford, K. M. Tyner, B. J. Dair, J. R. Deschamps and I. L. Medintz, *Anal. Chem.* 2011, **83**, 4453.
- 5 M. De, S. S. Chou, H. M. Joshi and V. P. Dravid, *Adv. Drug Deliv. Rev.* 2011, **63**, 1282.
- 6 M. L. Etheridge, S. A. Campbell, A. G. Erdman, C. L. Haynes, S. M. Wolf and J. McCullough, *Nanomedicine* 2013, **9**, 1.
- 7 H. C. Fischer and W. C. W. Chan, *Curr. Opin. Biotech.* 2007, **18**, 565.
- 8 A. J. Meuler, M. A. Hillmyer, F. S. Bates, *Macromolecules* 2009, **42**, 7221.
- 9 B. J. Dair, C. C. Honeker, D. B. Alward, A. Avgeropoulos, N. Hadjichristidis, L. J. Fetters, M. Capel and E. L. Thomas, *Macromolecules* 1999, **32**, 8145.
- 10 H. Jinnai, Y. Nishikawa, R. J. Spontak, S. D. Smith, D. A. Agard and T. Hashimoto, *Phys. Rev. Lett.* 2000, **84**, 518.
- 11 A. J. Meuler, G. Fleury, M. A. Hillmyer and F. S. Bates, *Macromolecules* 2008, **41**, 5809.
- 12 J. Jung, H. W. Park, J. Lee, H. Huang, T. Chang, Y. Rho, M. Ree, H. Sugimon and H. Jinnai, *Soft Matter* 2011, **7**, 10424.
- 13 T. Hashimoto, K. Tsutsumi and Y. Funaki, *Langmuir* 1997, **13**, 6869.
- 14 M. Adachi, A. Okumura, E. Sivaniah and T. Hashimoto, *Macromolecules* 2006, **39**, 7352.
- 15 J. Kibsgaard, Z. B. Chen, B. N. Reinecke and T. F. Jaramillo, *Nat. Mater.* 2012, **11**, 963.
- 16 S. Y. Lin, J. G. Fleming, D. L. Hetherington, B. K. Smith, R. Biswas, K. M. Ho, M. M. Sigalas, W. Zubrzycki, S. R. Kurtz and J. Bur, *Nature* 1998, **394**, 251.
- 17 V. Saranathan, C. O. Osuji, S. G. J. Mochrie, H. Noh, S. Narayanan, A. Sandy, E. R. Dufresne and R. O. Prum, *Proc. Natl. Acad. Sci. USA* 2010, **107**, 11676.
- 18 V. Z.-H. Chan, J. Hoffrman, V. Y. Lee, H. Latrou, A. Avgeropoulos, N. Hadjichristidis, R. D. Miller and E. L. Thomas, *Science* 1999, **286**, 1716.
- 19 A. Nykanen, M. Nuopponen, A. Laukkanen, S. P. Hirvonen, M. Rytela, O. Turunen, H. Tenhu, R. Mezzenga, O. Ikkala and J. Ruokolainen, *Macromolecules* 2007, **40**, 5827.
- 20 H. J. Snaith and L. Schmidt-Mende, *Adv. Mater.* 2007, **19**, 3187.
- 21 X. Yang and J. Loos, *Macromolecules* 2007, **40**, 1353.
- 22 E. J. W. Crossland, M. Kamperman, M. Nedelcu, C. Ducati, U. Wiesner, D. Smilgies, G. E. S. Toombes, M. A. Hillmyer, S. Ludwigs, U. Steiner and H. J. Snaith, *Nano Lett.* 2009, **9**, 2807.
- 23 E. J. W. Crossland, M. Nedelcu, C. Ducati, S. Ludwigs, M. A. Hillmyer, U. Steiner and H. J. Snaith, *Nano Lett.* 2009, **9**, 2813.
- 24 D. Wei, M. R. J. Scherer, C. Bower, P. Andrew, T. Ryhanen and U. Steiner, *Nano Lett.* 2012, **12**, 1857.
- 25 M. R. J. Scherer and U. Steiner, *Nano Lett.* 2013, **13**, 3005.; J. G. Werner, T. N. Hoheisel and U. Wiesner, *ACS Nano* 2014, **8**, 731.
- 26 D. A. Hajduk, P. E. Harper, S. M. Gruner, C. C. Honeker, G. Kim, E. L. Thomas and L. J. Fetters, *Macromolecules* 1994, **27**, 4063.
- 27 M. F. Schulz, F. S. Bates, K. Almdal and K. Mortensen, *Phys. Rev. Lett.* 1994, **73**, 86.
- 28 M. W. Matsen and M. Schick, *Phys. Rev. Lett.* 1994, **72**, 2660.
- 29 A. H. Schoen, *NASA Tech. Note* 1970, **D-5541**.
- 30 Y. Mogi, H. Kotsuji, Y. Kaneko, K. Mori, Y. Matsushita and I. Noda, *Macromolecules* 1992, **25**, 5408.
- 31 Y. Mogi, K. Mori, Y. Matsushita and I. Noda, *Macromolecules* 1992, **25**, 5412.
- 32 Y. Mogi, M. Nomura, H. Kotsuji, K. Ohnishi, Y. Matsushita and I. Noda, *Macromolecules* 1994, **27**, 6755.
- 33 T. S. Bailey, C. M. Hardy, T. H., III Epps and F. S. Bates, *Macromolecules* 2002, **35**, 7007.
- 34 M. Takenaka, T. Wakada, S. Akasaka, S. Nishitsuji, K. Saijo, H. Shimizu, M. I. Kim and H. Hasegawa, *Macromolecules* 2007, **40**, 4399.
- 35 E. W. Cochran and F. S. Bates, *Phys. Rev. Lett.* 2004, **93**, 087802/1-087802/4.
- 36 A. F. Wells *Three-Dimensional Nets and Polyhedra*; John Wiley & Sons: New York, 1977.
- 37 W. Longley and T. J. McIntosh, *Nature* 1983, **303**, 612.
- 38 P. Mariani, V. Luzzati and H. Delacroix, *J. Mol. Biol.* 1988, **204**, 165.
- 39 J. M. Seddon, *Biochim. Biophys. Acta* 1990, **1031**, 1.
- 40 C. Y. Chu, W. F. Lin, J. C. Tsai, C. S. Lai, S. C. Lo, H. L. Chen and T. Hashimoto, *Macromolecules* 2012, **45**, 2471.
- 41 H. Jinnai and X. Jiang, *Curr. Opin. Solid State Mat. Sci.* 2013, **17**, 135.
- 42 J. C. Kuo, J. C. Tsai, T. M. Chung and R. M. Ho, *Macromolecules* 2006, **39**, 7520.
- 43 Ch. Broennimann, E. F. Eikenberry, B. Henrich, R. Horisberger, G. Huelsen, E. Pohl, B. Schmitt, C. Schulze-Briese, M. Suzuki, T. Tomizaki, H. Toyokawa and A. Wagner, *J. of Synchrotron Radiation* 2006, **13**, 120.
- 44 J. R. Kremer, D. N. Mastrorade and J. R. McIntosh, *J. Struct. Biol.* 1996, **116**, 71.
- 45 P. Gilbert, *J. Theor. Biol.* 1972, **36**, 105.
- 46 K. I. Winey, E. L. Thomas and L. J. Fetters, *Macromolecules* 1992, **25**, 422.
- 47 G. Natta, I. Pasquon and A. Zambelli, *J. Am. Chem. Soc.* 1962, **84**, 1488.
- 48 T. C. Clancy, M. Pütz, J. D. Weinhold, J. G. Curro and W. L. Mattice, *Macromolecules* 2000, **33**, 9452.
- 49 L. J. Fetters, D. J. Lohse and W. W. Graessley, *J. Polym. Sci., Part B: Polym. Phys.* 1999, **37**, 1023.
- 50 L. Zhu, S. Z. D. Cheng, B. H. Calhoun, Q. Ge, R. P. Quirk, E. L. Thomas, B. S. Hsiao, F. Yeh and B. Lotz, *Polymer* 2001, **42**, 5829.
- 51 A. D. Benedicto and D. O'Brien, *Macromolecules* 1997, **30**, 3395.
- 52 J. M. Seddon, J. L. Hogan, N. A. Warrender and E. Pebay-Peyroula, *Prog. Colloid. Polym. Sci.* 1990, **81**, 189.
- 53 E. L. Thomas, D. B. Alward, D. J. Kinning, D. C. Martin, Jr. D. L. Handlin and L. J. Fetters, *Macromolecules* 1986, **19**, 2197.
- 54 H. Hasegawa, H. Tanaka, K. Yamasaki and T. Hashimoto, *Macromolecules* 1987, **20**, 1651.
- 55 S. L. Aggarwal, *Polymer* 1976, **17**, 938.
- 56 H. Jinnai, H. Watashiba, T. Kajihara, M. Takahashi, *J. Chem. Phys.* 2003, **119**, 7554.
- 57 H. Jinnai, T. Kajihara, H. Watashiba, Y. Nishikawa and R. J. Spontak, *Phys. Rev. E Rapid Communications* 2001, **64**, 010803(R)-010806(R):069903(E).
- 58 M. W. Matsen, F. S. Bates, *Macromolecules* 1996, **29**, 7641.
- 59 M. W. Matsen and F. S. Bates, *J. Chem. Phys.* 1997, **106**, 2436.
- 60 G. E. Schröder-Turk, A. Fogden and S. T. Hyde, *Eur. Phys. J. B* 2007, **59**, 115.

Graphical contents entry



Using electron tomography, we present the first real-space observation of the thermodynamically stable ordered bicontinuous double diamond (OBDD) structure in a diblock copolymer composed of a stereoregular block. The OBDD structure underwent a thermally reversible transition to double gyroid upon heating, and the transition was accompanied with a slight reduction of domain spacing, as demonstrated both experimentally and theoretically.